Supplement of

Soil moisture-induced changes in land carbon sink projections in CMIP6

Lea M. Gabele[1], Petra Sieber[1], Laibao Liu[2], and Sonia I. Seneviratne[1]

[1]Institute for Atmospheric and Climate Science, Department of Environmental Systems Science, ETH Zurich, Zurich, Switzerland

[2]Department of Geography, University of Hong Kong, Hong Kong SAR, China

Correspondence: Lea M. Gabele (lea.gabele@usys.ethz.ch) and Petra Sieber (petra.sieber@env.ethz.ch)

Supplementary Table S1. Main features of the land carbon cycle components of the participating models of LFMIP.

Modelling group	CESM, USA	CMSS, Italy	IPSL, France	MPI-M, Germany
ESM	CESM2	CMCC-ESM2	IPSL-CM6A-LR	MPI-ESM1-2-LR
Atmosphere resolution	0.9° × 1.25°	0.9° × 1.25°	2.5° × 1.3°	1.8° × 1.8°
Land model component	CLM5	CLM4.5	ORCHIDEE, branch 2.0	JSBACH3.2
Number of live carbon pools	22	N/A	8	3
Number of dead carbon pools	7	N/A	3	18
Number of plant functional types (PFTs)	16	15	15	13
Fire	Yes	Yes	No	Yes
Dynamic vegetation cover	No	No	No	Yes
Nitrogen cycle	Yes	Yes	No	Yes
References	(Danabasoglu et al., 2020; Lawrence et al., 2019)	(Lovato et al., 2022)	(Boucher et al., 2020)	(Mauritsen et al., 2019)

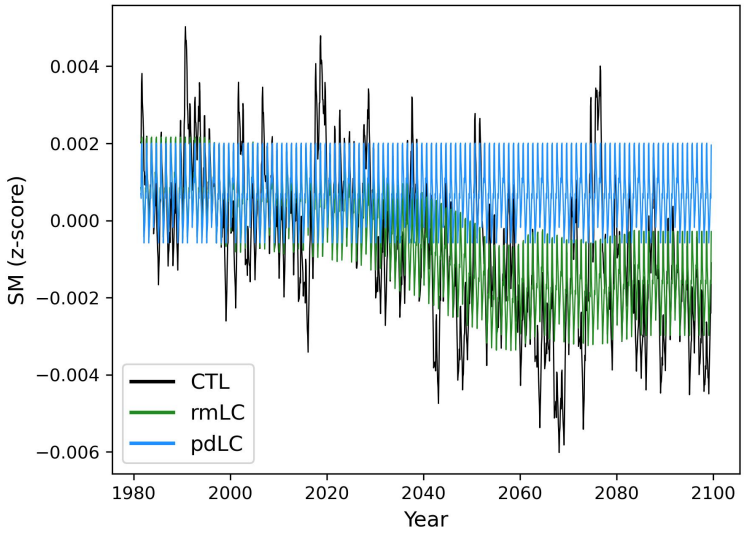

Supplementary Figure S1. Visualisation of the experiments of LFMIP (and GLACE-CMIP5), involving monthly SM from 1981 to 2099 for the reference run (CTL, black) and prescribed SM conditions for pdLC (blue) and rmLC (green) for a grid cell in South America (from CMCC-ESM2).

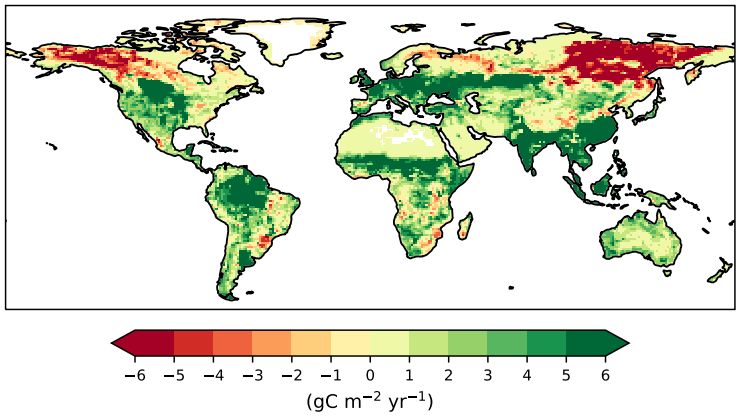

Supplementary Figure S2. Difference between the magnitudes of SM-induced change on GPP versus ecosystem respiration for the future period (2070-2099) for the LFMIP mean. Red indicates that SM has a stronger effect on ecosystem respiration and green indicates that SM has a stronger effect on GPP. White indicates no data.

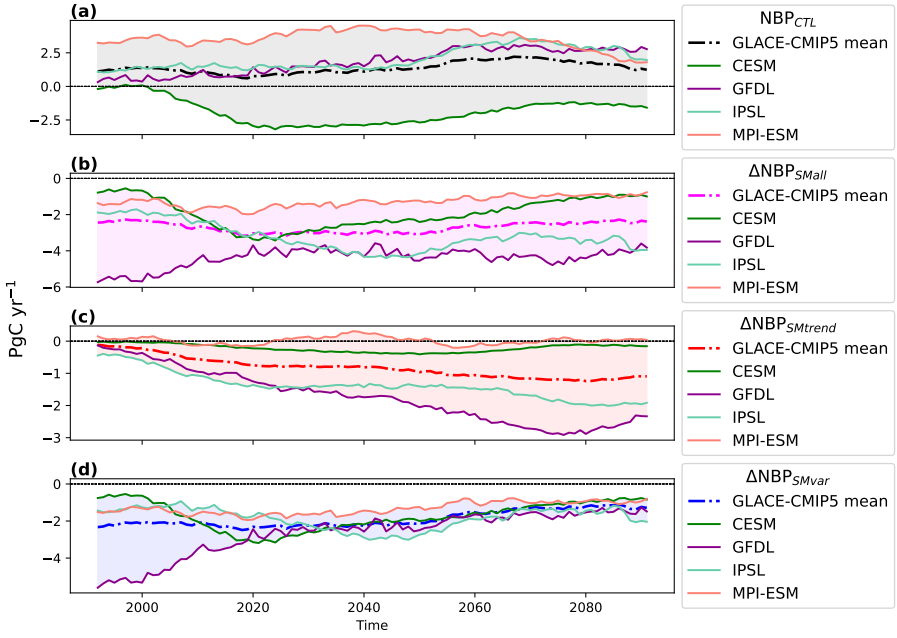

Supplementary Figure S3. Global evolution of (a) total NBP (NBP$_{CTL}$) for the GLACE-CMIP5 mean (black) and each GLACE model (CESM, GFDL, IPSL, and MPI-ESM), (b) the total SM effect on NBP (ΔNBP$_{SMall}$) for the GLACE-CMIP5 mean (red) and each GLACE-CMIP5 model, (c) the effect of SM trend on NBP (ΔNBP$_{SMtrend}$) for the GLACE-CMIP5 mean (red) and each GLACE-CMIP5 model, and (d) the effect of SM variability on NBP (ΔNBP$_{SMvar}$) for the GLACE-CMIP5 mean (blue) and each GLACE-CMIP5 model from 1991 to 2089 (smoothed with a 20 year centred rolling mean).

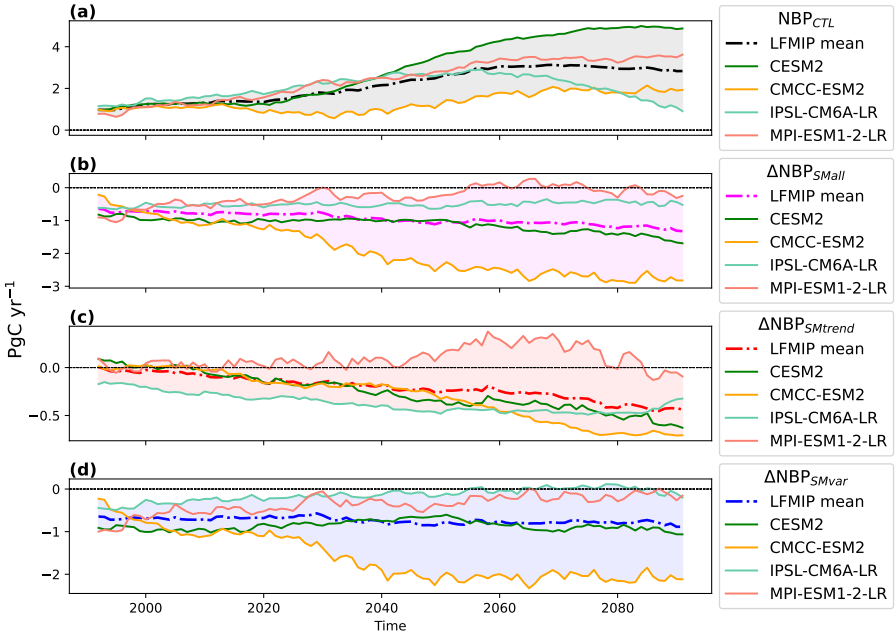

Supplementary Figure S4. Global evolution of (a) total NBP (NBP$_{CTL}$) for the LFMIP mean (black) and each LFMIP model (CESM, GFDL, IPSL, and MPI-ESM), (b) the total SM effect on NBP (ΔNBP$_{SMall}$) for the LFMIP mean (red) and each LFMIP model, (c) the effect of SM trend on NBP (ΔNBP$_{SMtrend}$) for the LFMIP mean (red) and each LFMIP model, and (d) the effect of SM variability on NBP (ΔNBP$_{SMvar}$) for the LFMIP mean (blue) and each LFMIP model from 1991 to 2089 (smoothed with a 20 year centred rolling mean).

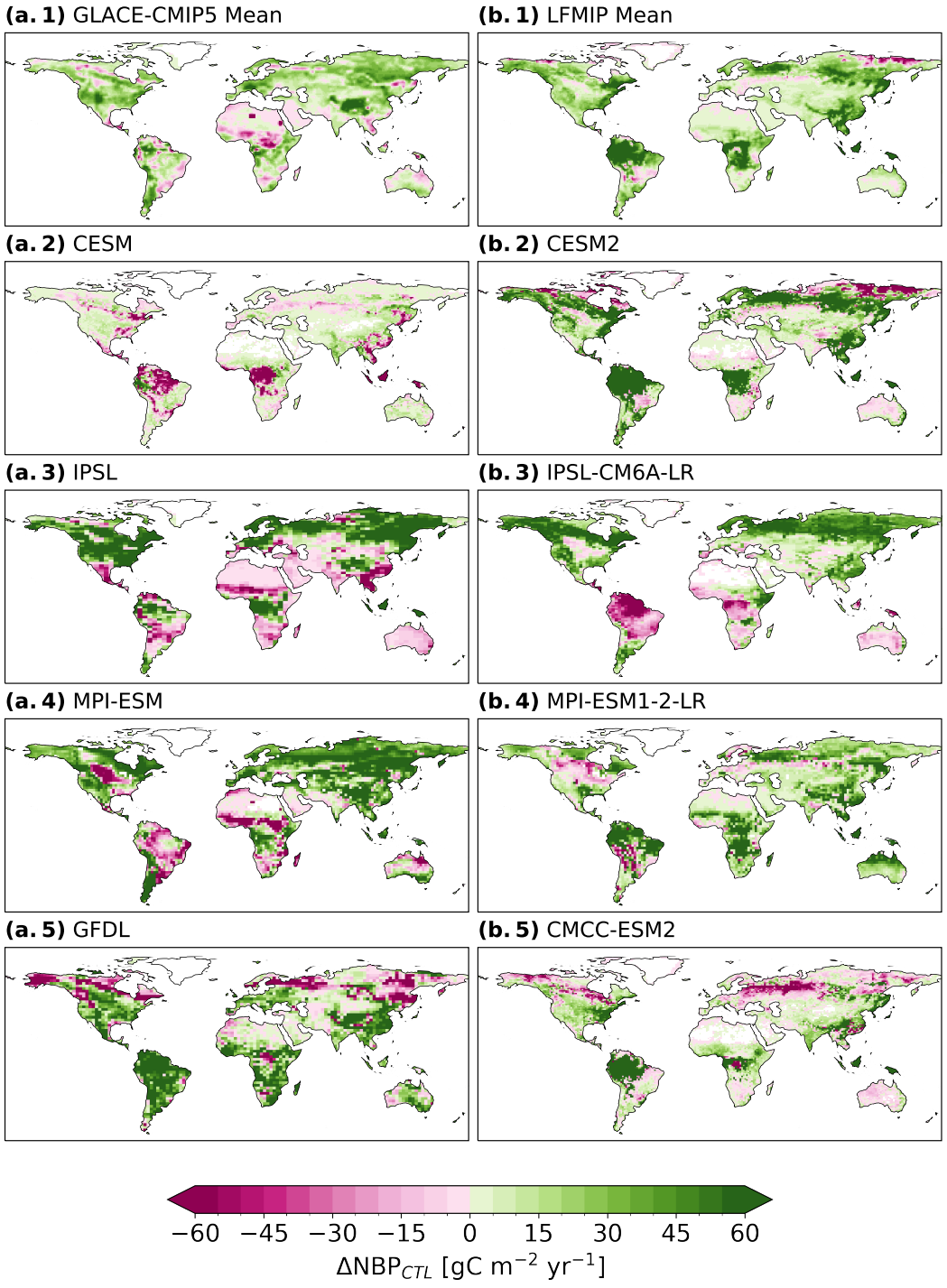

Supplementary Figure S5. NBP (NBP$_{CTL}$) for the future period (2070-2099) for (a.1) the GLACE-CMIP5 mean, (b.1) the LFMIP mean, (a.2-5) individual model projections of GLACE-CMIP5, and (b.2-5) individual model projections of LFMIP. Pink indicates a reduction and green an increase of NBP due to SM. White indicates no data.

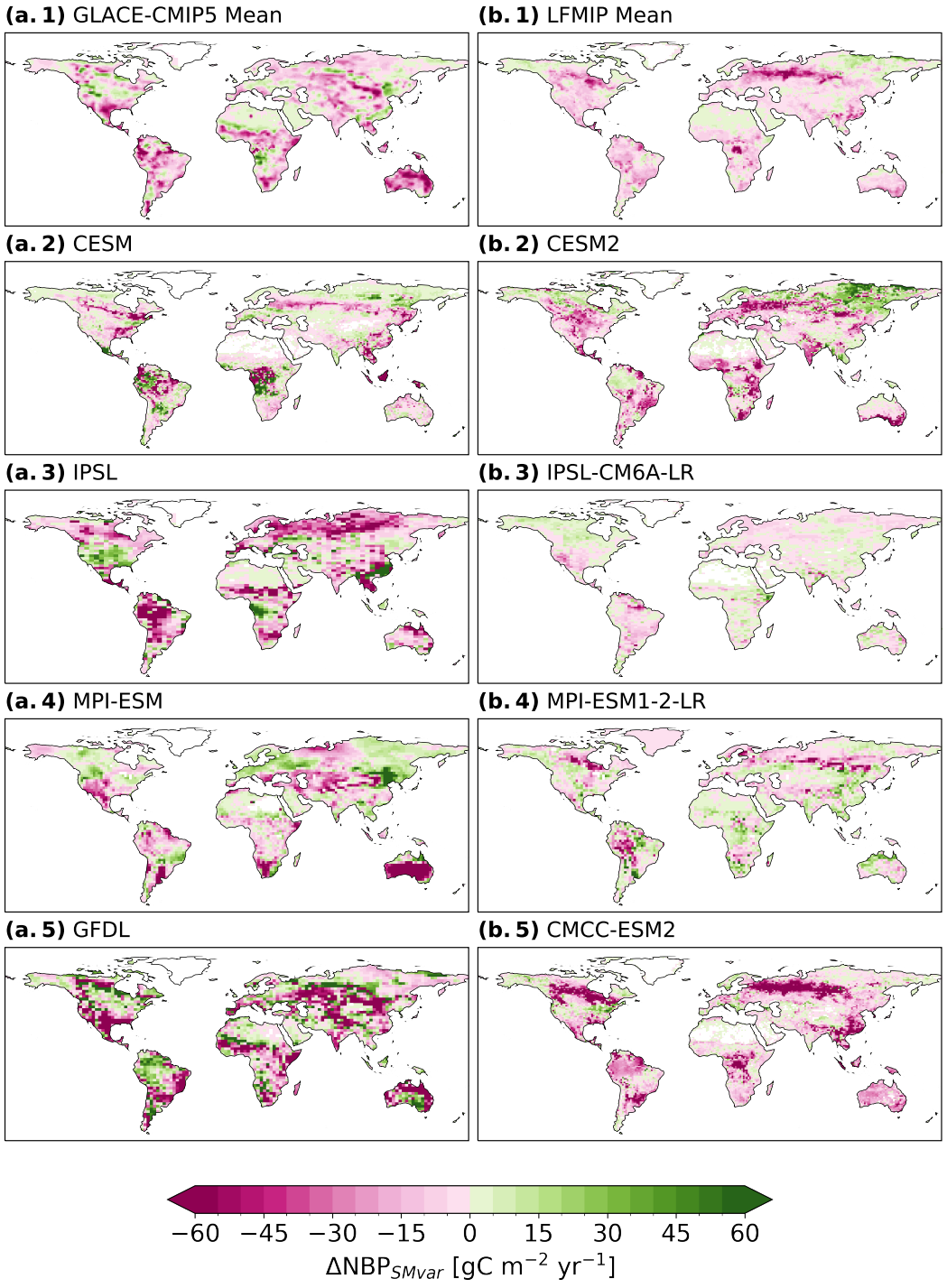

Supplementary Figure S6. Changes in NBP due to the effect of SM variability (ΔNBP_{SMvar}) for the future period (2070-2099) for (a.1) the GLACE-CMIP5 mean, (b.1) the LFMIP mean, (a.2-5) individual model projections of GLACE-CMIP5, and (b.2-5) individual model projections of LFMIP. Pink indicates a reduction and green an increase of NBP due to SM. White indicates no data.

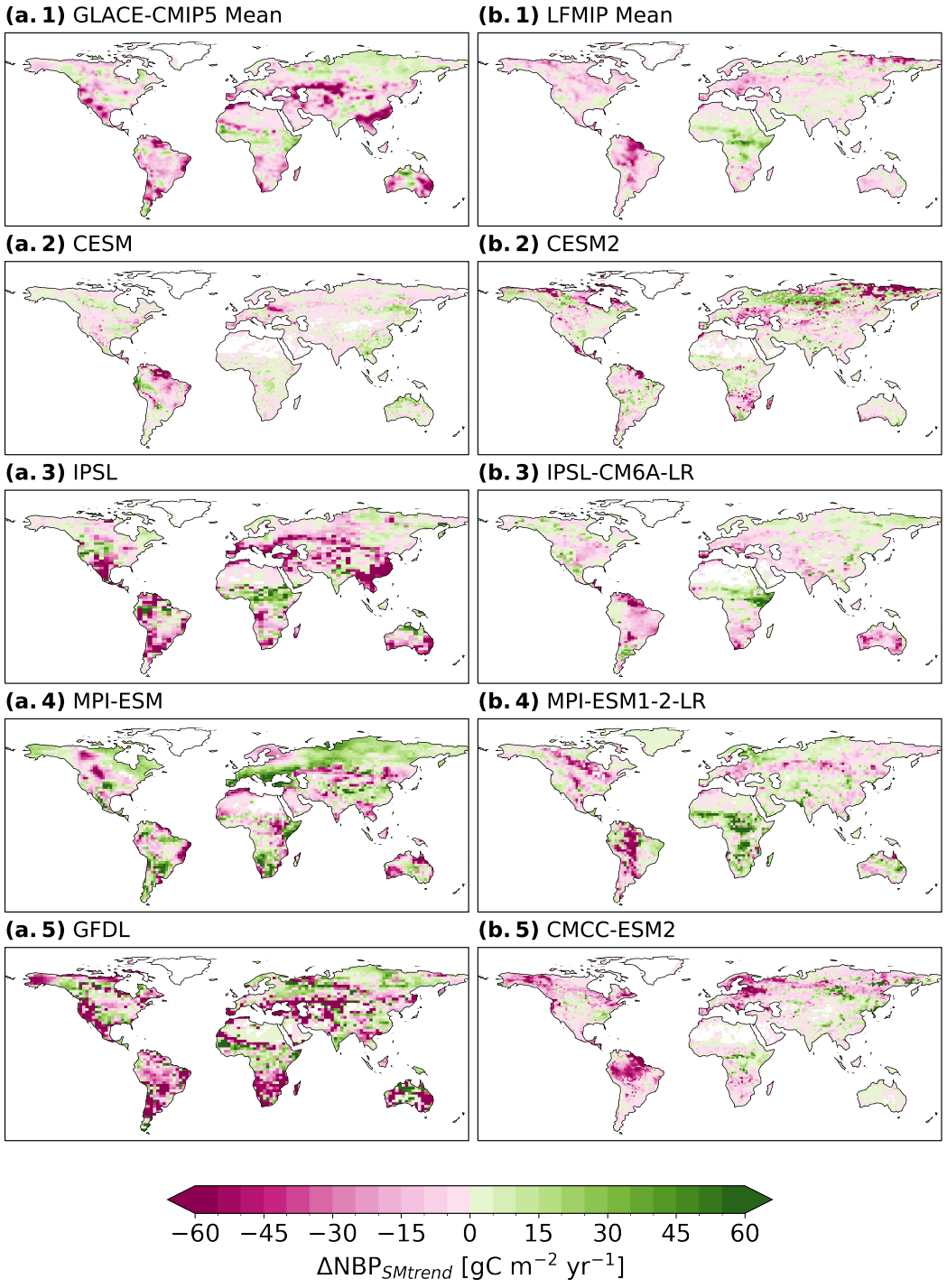

Supplementary Figure S7. Changes in NBP due to the effect of SM trend ($\Delta\text{NBP}_{SMtrend}$) for the future period (2070-2099) for (a.1) the GLACE-CMIP5 mean, (b.1) the LFMIP mean, (a.2-5) individual model projections of GLACE-CMIP5, and (b.2-5) individual model projections of LFMIP. Pink indicates a reduction and green an increase of NBP due to SM. White indicates no data.

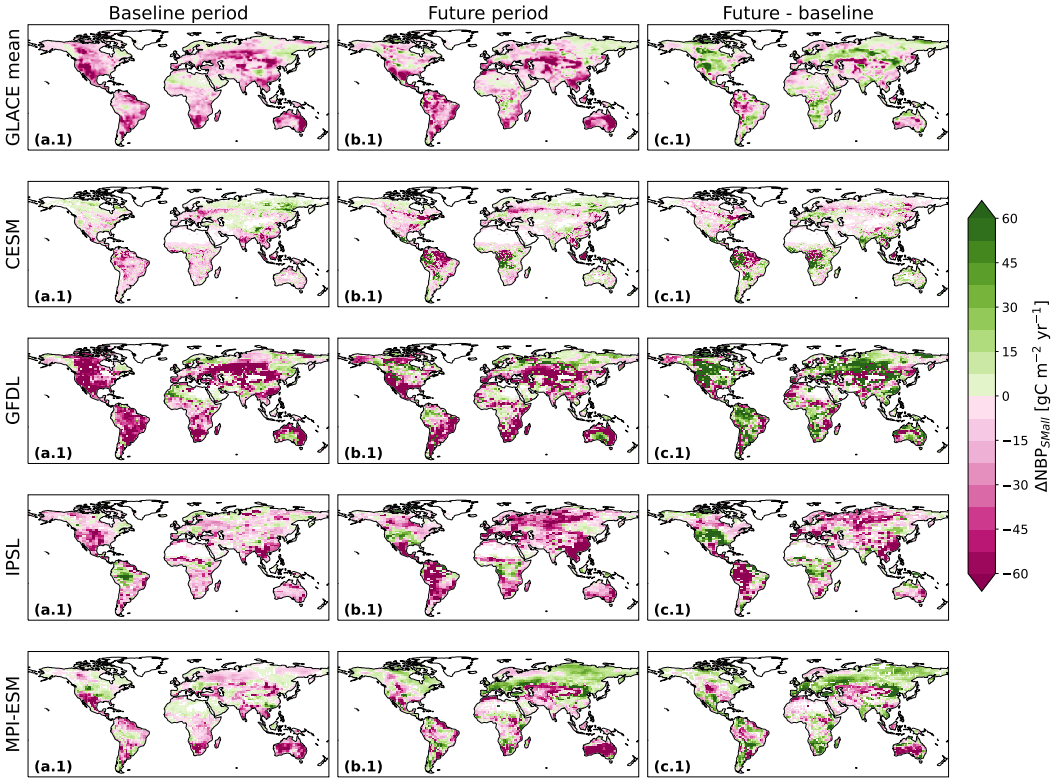

Supplementary Figure S8. Changes in NBP due to the total SM effect (ΔNBP_{SMall}) for (a) the present period (1980-2010), (b) the future period, and (c) the future period relative to the baseline for the GLACE-CMIP5 mean and the individual model projections of GLACE-CMIP5. Pink indicates a reduction and green an increase of NBP due to SM. White indicates no data.

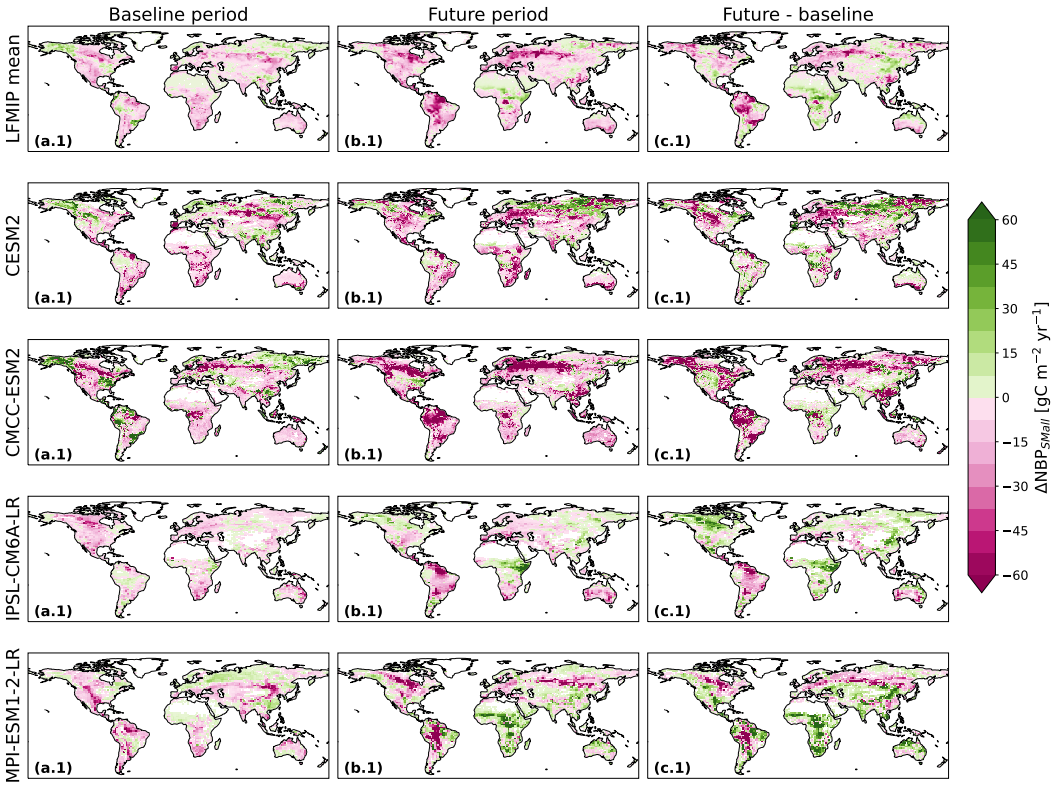

Supplementary Figure S9. Changes in NBP due to the total SM effect (ΔNBP_{SMall}) for (a) the present period (1980-2010), (b) the future period, and (c) the future period relative to the baseline for the LFMIP mean and the individual model projections of LFMIP. Pink indicates a reduction and green an increase of NBP due to SM. White indicates no data.

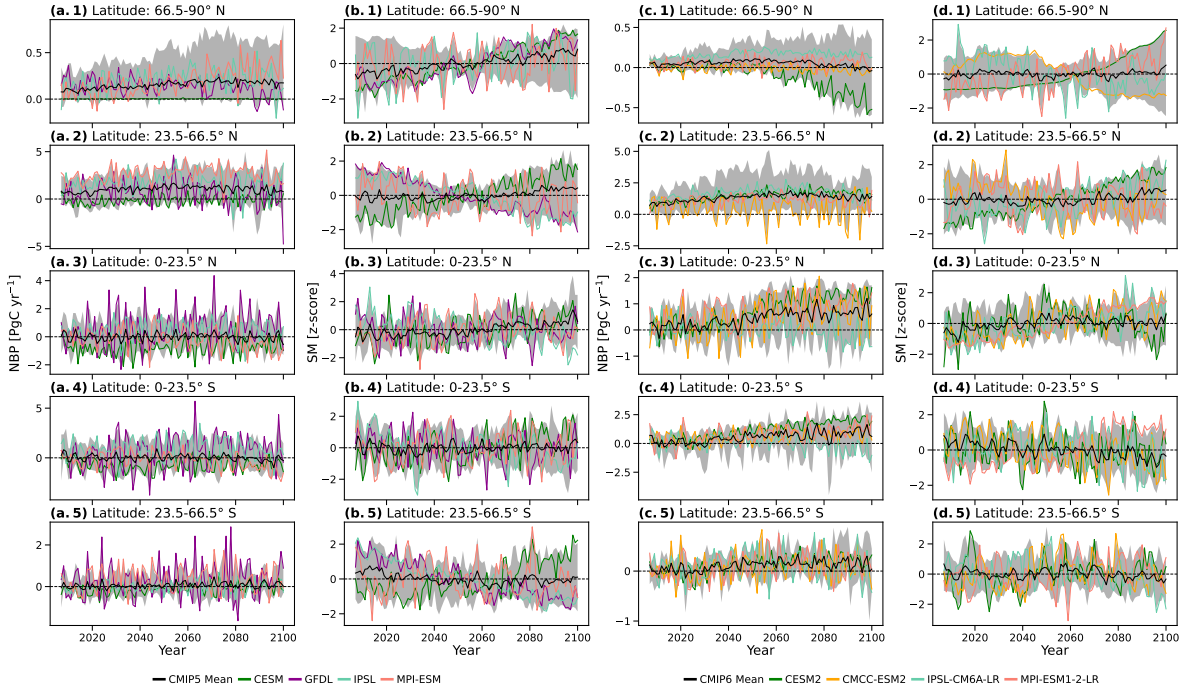

Supplementary Figure S10. Comparison of NBP and SM of (a, b) GLACE-CMIP5 to the CMIP5 multi-model mean (MMM) and (c, d) LFMIP to the CMIP6 MMM across latitudinal bands of 30° from north (1) to south (5). In columns (a) and (c), the coloured lines show latitudinal NBP for the GLACE-CMIP5 models, in columns (c) and (d), the coloured lines show latitudinal NBP for the GLACE-CMIP5 models. Black lines indicate the full ensemble MMMs and grey shadings the 95% confidence interval.

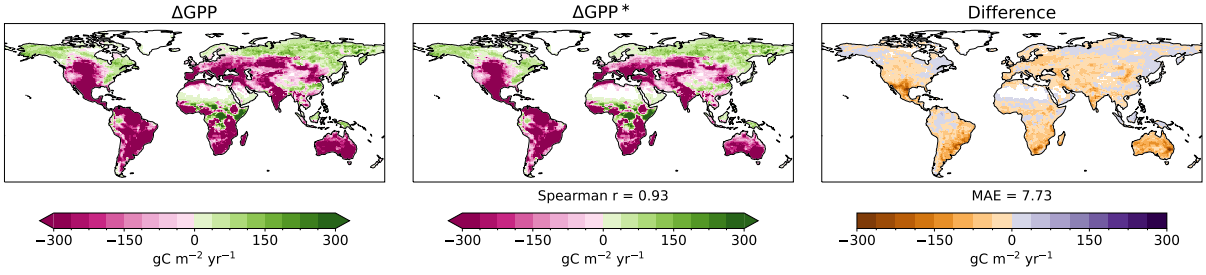

Supplementary Figure S11. Global changes in GPP due to the total SM effect modelled for the LFMIP mean (ΔGPP, left) and the LFMIP mean for the contribution analysis estimates (ΔGPP^*, middle), and the different between the modelled and the estimated total effect of SM on GPP (right) for future period (2070-2099). The pattern correlation (Spearman r) between the modelled and the estimated values is 0.93 and the mean absolute error (MAE) is 7.73 $gC\ m^{-2}\ yr^{-1}$.

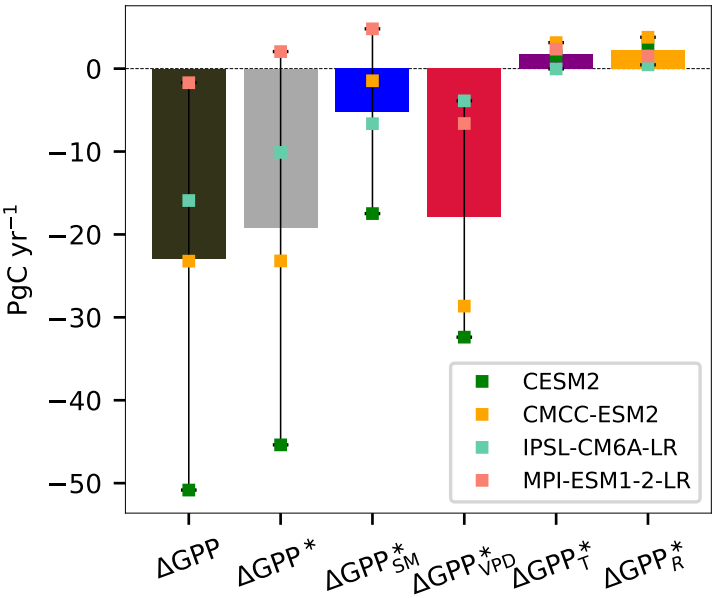

Supplementary Figure S12. Global changes in GPP due to the total SM effect modelled in LFMIP (ΔGPP, black bar). Contribution analysis estimates for LFMIP of the total global changes in GPP due to SM (ΔGPP^*, grey bar) and individual contributions from the direct SM effect (ΔGPP^*_{SM}, blue bar) and indirect SM effects via VPD (ΔGPP^*_{VPD}, light red bar), T (ΔGPP^*_T, purple bar) and R (ΔGPP^*_R, yellow bar) for the future period (2070-2099). Bars show the LFMIP mean and coloured dots the individual models.

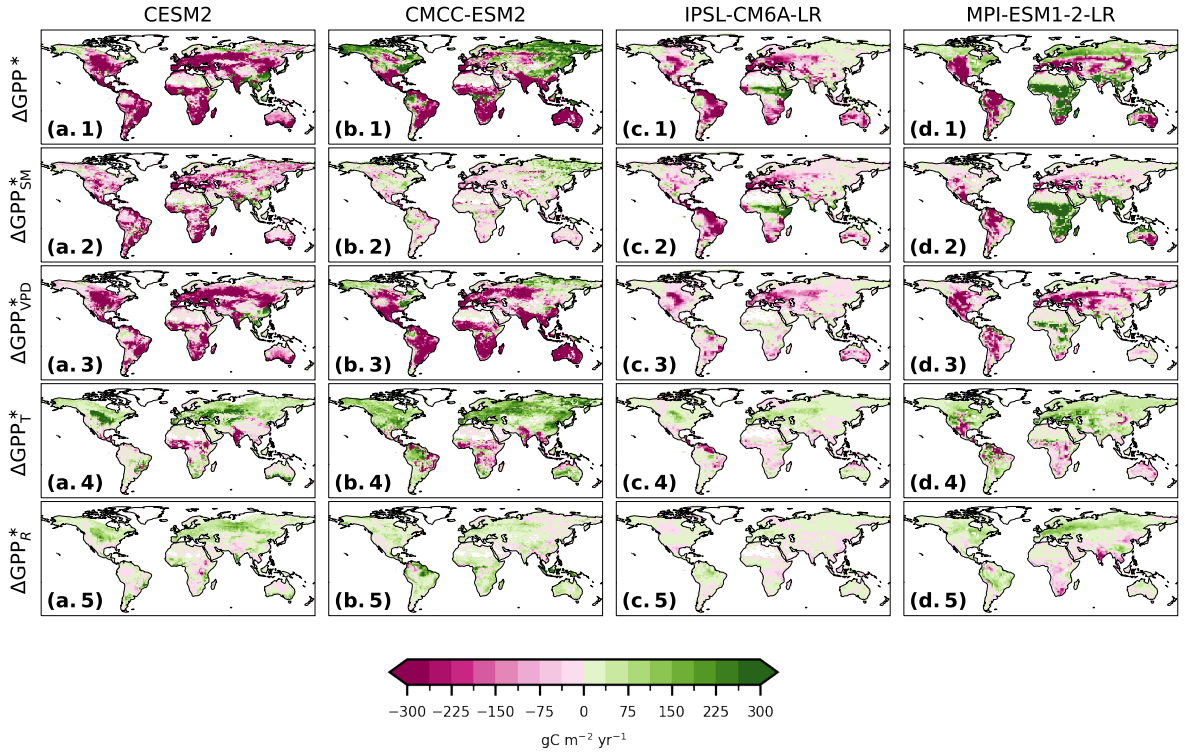

Supplementary Figure S13. Contribution analysis estimate for LFMIP of the total changes in GPP due to SM (ΔGPP^*) and the individual contributions from the direct SM effect (ΔGPP^*_{SM}), the indirect SM effects via VPD (ΔGPP^*_{VPD}, light red bar), T (ΔGPP^*_T, purple bar) and R (ΔGPP^*_R, yellow bar) for the future period (2070-2099). Pink indicates a reduction and green an increase of NBP due to SM. White indicates no data.

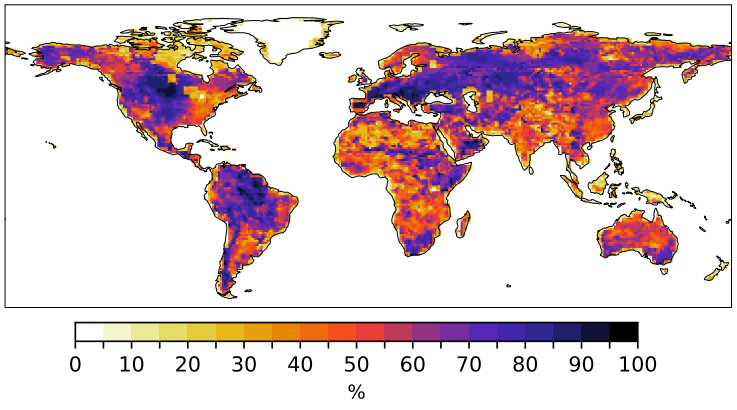

Supplementary Figure S14. Total fraction of intermodel differences attributed to the disagreement in the sensitivity of GPP to SM and differences in the change in SM by the factorial ANOVA variance decomposition for LFMIP (in %).

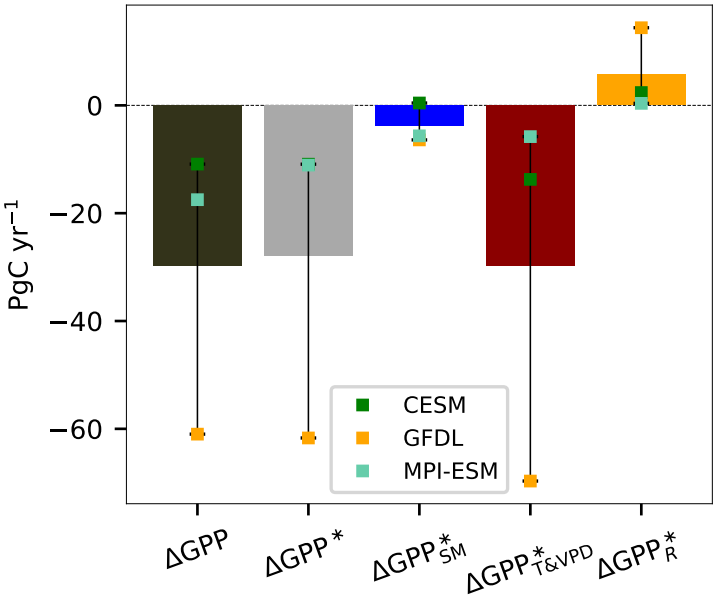

Supplementary Figure S15. Global changes in GPP due to the total SM effect modelled in GLACE-CMIP5 (ΔGPP, black bar). Contribution analysis estimates for GLACE-CMIP5 of the total global changes in GPP due to SM (ΔGPP^*, grey bar) and individual contributions from the direct SM effect (ΔGPP^*_{SM}, blue bar) and indirect SM effects via VPD and T ($\Delta GPP^*_{T\&VPD}$, red bar) and R (ΔGPP^*_R, yellow bar) for the future period (2070-2099). Bars show the LFMIP mean and coloured dots the individual models. For GLACE-CMIP5 model output is only available for CESM, GFDL, and MPI-ESM.

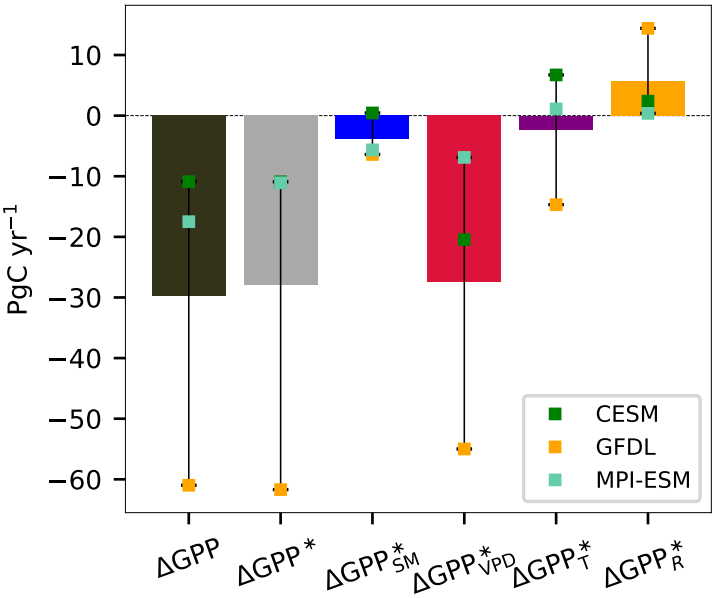

Supplementary Figure S16. Global changes in GPP due to the total SM effect modelled in GLACE-CMIP5 (ΔGPP, black bar). Contribution analysis estimates for GLACE-CMIP5 of the total global changes in GPP due to SM (ΔGPP^*, grey bar) and individual contributions from the direct SM effect (ΔGPP^*_{SM}, blue bar) and indirect SM effects via VPD (ΔGPP^*_{VPD}, light red bar), T (ΔGPP^*_T, purple bar) and R (ΔGPP^*_R, yellow bar) for the future period (2070-2099). Bars show the LFMIP mean and coloured dots the individual models. For GLACE-CMIP5 model output is only available for CESM, GFDL, and MPI-ESM.

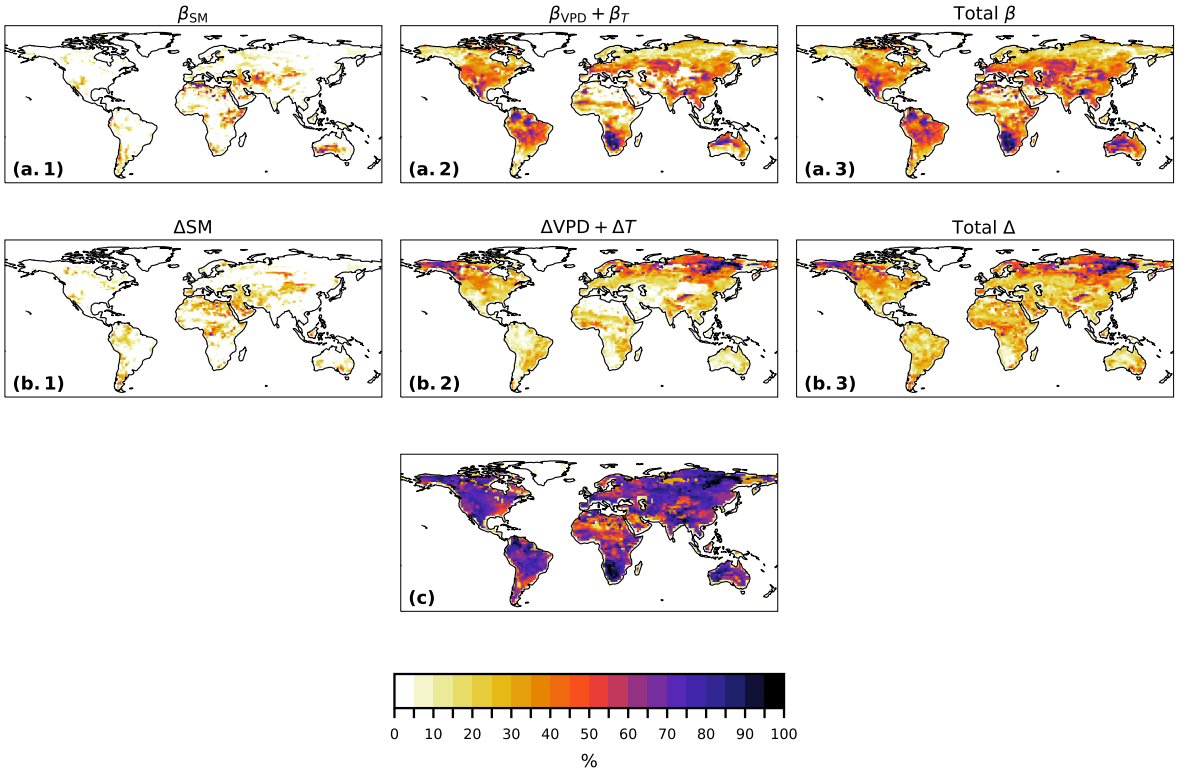

Supplementary Figure S17. Contribution to intermodel differences (in %) in GLACE-CMIP5 from disagreement in the sensitivity of GPP to (a.1) the direct SM effect (β_{SM}), (a.2) indirect SM effects via T and VPD (β_{VPD} + β_T) and (a.3) direct and indirect SM effects (Total β), as well as contribution from (b.1) the change in SM (ΔSM), (b.2) the change in T and VPD due to SM ($\Delta VPD + \Delta T$), and (b.3) the total contribution of change in SM (Total Δ). (c) shows the total fraction of intermodel differences attributed to the disagreement in the sensitivity of GPP to SM and differences in the change in SM.

References

Boucher, O., Servonnat, J., Albright, A. L., Aumont, O., Balkanski, Y., Bastrikov, V., Bekki, S., Bonnet, R., Bony, S., Bopp, L., Braconnot, P., Brockmann, P., Cadule, P., Caubel, A., Cheruy, F., Codron, F., Cozic, A., Cugnet, D., D'Andrea, F., Davini, P., de Lavergne, C., Denvil, S., Deshayes, J., Devilliers, M., Ducharne, A., Dufresne, J. L., Dupont, E., Éthé, C., Fairhead, L., Falletti, L., Flavoni, S., Foujols, M. A., Gardoll, S., Gastineau, G., Ghattas, J., Grandpeix, J. Y., Guenet, B., Guez, E., L., Guilyardi, E., Guimberteau, M., Hauglustaine, D., Hourdin, F., Idelkadi, A., Joussaume, S., Kageyama, M., Khodri, M., Krinner, G., Lebas, N., Levavasseur, G., Lévy, C., Li, L., Lott, F., Lurton, T., Luyssaert, S., Madec, G., Madeleine, J. B., Maignan, F., Marchand, M., Marti, O., Mellul, L., Meurdesoif, Y., Mignot, J., Musat, I., Ottlé, C., Peylin, P., Planton, Y., Polcher, J., Rio, C., Rochetin, N., Rousset, C., Sepulchre, P., Sima, A., Swingedouw, D., Thiéblemont, R., Traore, A. K., Vancoppenolle, M., Vial, J., Vialard, J., Viovy, N., and Vuichard, N.: Presentation and Evaluation of the IPSL-CM6A-LR Climate Model, Journal of Advances in Modeling Earth Systems, 12, https://doi.org/10.1029/2019MS002010, publisher: Blackwell Publishing Ltd, 2020.

Danabasoglu, G., Lamarque, J. F., Bacmeister, J., Bailey, D. A., DuVivier, A. K., Edwards, J., Emmons, L. K., Fasullo, J., Garcia, R., Gettelman, A., Hannay, C., Holland, M. M., Large, W. G., Lauritzen, P. H., Lawrence, D. M., Lenaerts, J. T., Lindsay, K., Lipscomb, W. H., Mills, M. J., Neale, R., Oleson, K. W., Otto-Bliesner, B., Phillips, A. S., Sacks, W., Tilmes, S., van Kampenhout, L., Vertenstein, M., Bertini, A., Dennis, J., Deser, C., Fischer, C., Fox-Kemper, B., Kay, J. E., Kinnison, D., Kushner, P. J., Larson, V. E., Long, M. C., Mickelson, S., Moore, J. K., Nienhouse, E., Polvani, L., Rasch, P. J., and Strand, W. G.: The Community Earth System Model Version 2 (CESM2), Journal of Advances in Modeling Earth Systems, 12, https://doi.org/10.1029/2019MS001916, publisher: Blackwell Publishing Ltd, 2020.

Lawrence, D. M., Fisher, R. A., Koven, C. D., Oleson, K. W., Swenson, S. C., Bonan, G., Collier, N., Ghimire, B., van Kampenhout, L., Kennedy, D., Kluzek, E., Lawrence, P. J., Li, F., Li, H., Lombardozzi, D., Riley, W. J., Sacks, W. J., Shi, M., Vertenstein, M., Wieder, W. R., Xu, C., Ali, A. A., Badger, A. M., Bisht, G., van den Broeke, M., Brunke, M. A., Burns, S. P., Buzan, J., Clark, M., Craig, A., Dahlin, K., Drewniak, B., Fisher, J. B., Flanner, M., Fox, A. M., Gentine, P., Hoffman, F., Keppel-Aleks, G., Knox, R., Kumar, S., Lenaerts, J., Leung, L. R., Lipscomb, W. H., Lu, Y., Pandey, A., Pelletier, J. D., Perket, J., Randerson, J. T., Ricciuto, D. M., Sanderson, B. M., Slater, A., Subin, Z. M., Tang, J., Thomas, R. Q., Val Martin, M., and Zeng, X.: The Community Land Model Version 5: Description of New Features, Benchmarking, and Impact of Forcing Uncertainty, Journal of Advances in Modeling Earth Systems, 11, 4245–4287, https://doi.org/10.1029/2018MS001583, publisher: Blackwell Publishing Ltd, 2019.

Lovato, T., Peano, D., Butenschön, M., Materia, S., Iovino, D., Scoccimarro, E., Fogli, P. G., Cherchi, A., Bellucci, A., Gualdi, S., Masina, S., and Navarra, A.: CMIP6 Simulations With the CMCC Earth System Model (CMCC-ESM2), Journal of Advances in Modeling Earth Systems, 14, https://doi.org/10.1029/2021MS002814, publisher: John Wiley and Sons Inc, 2022.

Mauritsen, T., Bader, J., Becker, T., Behrens, J., Bittner, M., Brokopf, R., Brovkin, V., Claussen, M., Crueger, T., Esch, M., Fast, I., Fiedler, S., Fläschner, D., Gayler, V., Giorgetta, M., Goll, D. S., Haak, H., Hagemann, S., Hedemann, C., Hohenegger, C., Ilyina, T., Jahns, T., Jimenéz-de-la Cuesta, D., Jungclaus, J., Kleinen, T., Kloster, S., Kracher, D., Kinne, S., Kleberg, D., Lasslop, G., Kornblueh, L., Marotzke, J., Matei, D., Meraner, K., Mikolajewicz, U., Modali, K., Möbis, B., Müller, W. A., Nabel, J. E., Nam, C. C., Notz, D., Nyawira, S. S., Paulsen, H., Peters, K., Pincus, R., Pohlmann, H., Pongratz, J., Popp, M., Raddatz, T. J., Rast, S., Redler, R., Reick, C. H., Rohrschneider, T., Schemann, V., Schmidt, H., Schnur, R., Schulzweida, U., Six, K. D., Stein, L., Stemmler, I., Stevens, B., von Storch, J. S., Tian, F., Voigt, A., Vrese, P., Wieners, K. H., Wilkenskjeld, S., Winkler, A., and Roeckner, E.: Developments in the MPI-M Earth System

Model version 1.2 (MPI-ESM1.2) and Its Response to Increasing CO2, Journal of Advances in Modeling Earth Systems, 11, 998–1038, https://doi.org/10.1029/2018MS001400, publisher: Blackwell Publishing Ltd, 2019.